IMPACT OF THE PARALLEL IMAGING RECONSTRUCTION ALGORITHM ON BRAIN ACTIVITY DETECTION IN FMRI

Lotfi Chaâri[1,2]*, Sébastien Mériaux*[2]*, Jean-Christophe Pesquet*[1] *and Philippe Ciuciu*[2]

[1] Université Paris-Est, IGM and UMR-CNRS 8049,
77454 Marne-la-Vallée cedex, France
{chaari,pesquet}@univ-mlv.fr

[2] CEA/DSV/I^{2}BM/Neurospin, CEA Saclay, Bbt. 145,
Point Courrier 156, 91191 Gif-sur-Yvette cedex, France
{sebastien.meriaux,philippe.ciuciu}@cea.fr

ABSTRACT

PMRI is a fast imaging technique that allows reconstruction of full FoV images based on undersampled k-space data acquired using multiple reciever coils with complementary sensitivity profiles. It enables the acquisition of highly resolved images either in space or in time, which is of particular interest in applications like neuroimaging. These improvements are counterbalanced by a degraded SNR and the presence of artifacts that depend on the reconstruction algorithm. To improve the performance of the widely used SENSE algorithm, regularization in the wavelet domain has been efficiently investigated. In this paper, we illustrate the gain induced by such a regularization in terms of statistical impact on fMRI data analysis using a fast-event related protocol. Our results show that the reconstruction algorithm has a dramatic impact on the statistical sensitivity in fMRI and that the proposed method outperforms classical SENSE reconstruction at the subject-level using different acquisition setups.

1 Introduction

Parallel imaging in Magnetic Resonance Imaging (pMRI) aims at reducing acquisition time in clinical applications or at improving spatial or temporal resolution of acquired images in neuroimaging. Many methods like GRAPPA (Generalized Autocalibrating Partially Parallel Acquisitions) [1] and SENSE (Sensitivity Encoding) [2] have been proposed in the literature to reconstruct a full Field of View (FoV) image from multiple k-space undersampled images acquired on separate channels. GRAPPA-based reconstruction operates in the k-space, while SENSE proceeds in the image domain (after an inverse Fourier transform of reduced FoV images). Another difference is that GRAPPA is autocalibrated, while SENSE needs a separate coil sensitivity estimation step based on a reference scan. Note however that an autocalibrated version of SENSE is also available for instance in Siemens scanners and called mSENSE hereafter. All these methods may suffer from strong artifacts when high values of acceleration factors R are considered in the imaging setup or when they are applied to Echo Planar Images (EPI), which are acquired during fMRI experiments. These artifacts can drastically disturb subsequent analysis such as brain activation detection in functional neuroimaging. Regularized SENSE methods have been proposed in the literature to improve the robustness of the solution [3–8], some of them apply quadratic regularization while others resort to regularization in the wavelet transform domain. To the best of our knowledge no study has been conducted to assess the impact of using a specific pMRI reconstruction algorithm on brain activation detection in fMRI. There are several underlying reasons: first, all pMRI algorithms are not available on a specific scanner. Second, reconstructing the full FoV image with an external pMRI algorithm requires to get and read the huge raw data files from the MRI scanner, then reconstruct all reduced FoV images using a *home-made* reconstruction pipeline that embodies ghosting EPI artifact corrections and k-space regridding, before applying the proposed pMRI method to each volume of the fMRI series. The goal of this study is therefore to fill this gap and to compare different SENSE-based reconstruction algorithms [4, 6] quantitatively. More specifically, we aim at demonstrating that a significant gain in spatial in-plane resolution ($2 \times 2\text{mm}^2$) can be achieved using $R = 2$ at a constant time of repetition (TR, ie the between-scan time interval) without sacrificing the statistical sensitivity if a wavelet-based regularized algorithm is involved in the pipeline. Our EPI fMRI data are acquired during a cognitive event-related protocol. After volume by volume pMRI reconstruction by the different algorithms, our comparison thus takes place at statistical analysis step to derive quantitative comparison criteria (voxel-level and cluster-level corrected p-values and T-scores). To this end, the reconstructed full FoV images are analysed in the General Linear Model (GLM) framework using SPM5 [1]. Our particular interest is to demonstrate that when artifacts are superimposed to brain activation, this directly impacts subsequent statistical analysis. Also, our analysis is conducted at the subject-

[1] `http://www.fil.ion.ucl.ac.uk`

level in order to avoid normalization artifacts induced by multi-subject registration in group studies.
The rest of the paper is organized as follows. In Section 2, we briefly recall the pMRI background. Section 3 is devoted to the SENSE algorithm and its regularized version in the wavelet transform domain. In Section 4, qualitative and quantitative illustrations show the impact of the proposed wavelet-based regularized reconstruction on brain activation detection. Finally, conclusions and perspectives are drawn in Section 5.

2 Parallel imaging in MRI

In parallel MRI, an array of L coils is employed to measure the spin density $\overline{\rho}$ into the object under investigation.[2] The signal $\widetilde{d}_\ell$ received by each coil ℓ is the Fourier transform of the desired 2D field $\overline{\rho} \in \mathbb{R}^{Y \times X}$ on the specified FoV weighted by the coil sensitivity profile s_ℓ, evaluated at some location $\boldsymbol{k}_r = (k_y, k_x)^\intercal$ in the k-space:

$$\widetilde{d}_\ell(\boldsymbol{k}_r) = \int \overline{\rho}(\boldsymbol{r}) s_\ell(\boldsymbol{r}) e^{-\imath 2\pi \boldsymbol{k}_r^\intercal \boldsymbol{r}}\, d\boldsymbol{r} + \widetilde{n}_\ell(\boldsymbol{k}_r), \qquad (1)$$

where $\widetilde{n}_\ell(\boldsymbol{k}_r)$ is a coil-dependent additive zero-mean Gaussian noise, which is independent and identically distributed (iid) in the k-space, and $\boldsymbol{r} = (y, x)^\intercal \in Y \times X$ is the spatial position in the image domain. For the sake of simplicity, a Cartesian coordinate system is generally adopted in neuroimaging. In parallel MRI, the sampling period along the phase encoding direction is R times larger than the one used for conventional acquisition, $R \leq L$ being the reduction factor. To recover full FoV images, an unfolding step has to be performed. In what follows, we focus on SENSE-like methods operating in the space domain. A 2D inverse Fourier transform allows us first to recover the measured signal in the spatial domain. By accounting for the k-space undersampling at R rate, the inverse Fourier transform gives us the spatial counterpart of Eq. (1) in matrix form [6]:

$$\boldsymbol{d}(\boldsymbol{r}) = \boldsymbol{S}(\boldsymbol{r}) \overline{\boldsymbol{\rho}}(\boldsymbol{r}) + \boldsymbol{n}(\boldsymbol{r}), \qquad (2)$$

where $\overline{\boldsymbol{\rho}}(\boldsymbol{r}) \triangleq [\overline{\rho}(y, x), .., \overline{\rho}(y + (R-1)\Delta y, x)]^\intercal$,

$$\boldsymbol{S}(\boldsymbol{r}) \triangleq \begin{bmatrix} s_1(y,x) & \dots & s_1(y+(R-1)\Delta y, x) \\ \vdots & \vdots & \vdots \\ s_L(y,x) & \dots & s_L(y+(R-1)\Delta y, x) \end{bmatrix},$$

$\boldsymbol{d}(\boldsymbol{r}) \triangleq [d_1(y,x), .., d_L(y,x)]^\intercal$, $\boldsymbol{n}(\boldsymbol{r}) \triangleq [n_1(y,x), .., n_L(y,x)]^\intercal$, $\Delta y = \frac{Y}{R}$ being the aliasing period and y and x the position in the image domain along the phase and encoding directions, respectively. Based on this model, the reconstruction step consists of solving Eq. (2) and recovering $\overline{\boldsymbol{\rho}}(\boldsymbol{r})$ from $\boldsymbol{d}(\boldsymbol{r})$ and an $\boldsymbol{S}(\boldsymbol{r})$ at each spatial positions $\boldsymbol{r} = (y, x)^\intercal$. The spatial mixture or *sensitivity* matrix $\boldsymbol{S}(\boldsymbol{r})$ is estimated using a reference scan and varies according to the coil geometry. Note that the coil images $(d_\ell)_{1 \leq l \leq L}$ as well as the sought image $\overline{\rho}$ are complex-valued, although $|\overline{\rho}|$ is only considered for visualization.

[2] The overbar is used to distinguish the "true" data from a generic variable.

3 Reconstruction algorithms

For the sake of conciseness, all pMRI reconstruction algorithms considered here minimize an objective function of the following form:

$$\mathcal{J}(\rho) = \sum_{\mathbf{r}} \| \boldsymbol{d}(\boldsymbol{r}) - \boldsymbol{S}(\boldsymbol{r}) \boldsymbol{\rho}(\boldsymbol{r}) \|^2_{\boldsymbol{\Psi}^{-1}} + \kappa_1 \Phi(\rho) + \kappa_2 i_{\mathcal{M}}(\rho), \qquad (3)$$

where $\kappa_1, \kappa_2 \geq 0$ are two constants, and Φ and $i_{\mathcal{M}}$ are two functions to be specified. The noise covariance matrix $\boldsymbol{\Psi}$ is usually estimated based on L acquired images $(\underline{\mathrm{d}}_\ell)_{1 \leq \ell \leq L}$ from all coils without radio frequency pulses. In this paper, we are interested in reconstructing one slice (2D image). To reconstruct a full volume, the detailed algorithms hereafter have to be iterated over slices.

3.1 1D-SENSE

In its simplest form, SENSE imaging amounts to solving a one-dimensional inversion problem due to the separability of the Fourier transform. Note however that this inverse problem admits a two-dimensional extension in 3D imaging sequences like Echo Volume Imaging (EVI) [9] where undersampling occurs in two k-space directions. The 1D-SENSE reconstruction [2] actually minimizes a Weighted Least Squares (WLS) criterion $\mathcal{J}_{\mathrm{WLS}}$ which can be derived by setting $\kappa_1 = \kappa_2 = 0$ in Eq. (3). Hence, the SENSE full FoV image is simply the maximum likelihood estimate under Gaussian noise assumptions and admits the following closed-form expression at each spatial position $\boldsymbol{r}$:

$$\widehat{\boldsymbol{\rho}}_{\mathrm{WLS}}(\boldsymbol{r}) = \left(\boldsymbol{S}^{\mathsf{H}}(\boldsymbol{r}) \boldsymbol{\Psi}^{-1} \boldsymbol{S}(\boldsymbol{r})\right)^{\sharp} \boldsymbol{S}^{\mathsf{H}}(\boldsymbol{r}) \boldsymbol{\Psi}^{-1} \boldsymbol{d}(\boldsymbol{r}), \qquad (4)$$

where $(\cdot)^{\mathsf{H}}$ (resp. $(\cdot)^{\sharp}$) stands for the transposed complex conjugate (resp. pseudo-inverse). In practice, the performance of the 1D-SENSE method is limited because of the presence of *i)* distortions in the measurements $\boldsymbol{d}(\boldsymbol{r})$, *ii)* the putative ill-conditioning of $\boldsymbol{S}(\boldsymbol{r})$ at locations $\boldsymbol{r}$ close to the image center and *iii)* the presence of errors in the estimation of $\boldsymbol{S}(\boldsymbol{r})$ mainly at brain/air interfaces. To improve the robustness of the solution to this ill-posed problem, regularization is usually used. As investigated by *Chaâri et al.* [6,8] and *Liu et al.* [7], regularization in the Wavelet Transform (WT) domain is a powerful tool to improve SENSE reconstruction. In what follows, we summarize the wavelet-based regularization approach.

3.2 1D-UWR-SENSE

Let T be the WT operator which corresponds to a discrete decomposition onto a separable 2D dyadic orthonormal wavelet basis performed over $j_{\max}$ resolution levels. The full FoV image $\overline{\rho}$ of size $Y \times X$ can be seen as an element of the Euclidean space $\mathbb{C}^K$ with $K = Y \times X$ endowed with the standard inner product $\langle \cdot \mid \cdot \rangle$ and norm $\| \cdot \|$. The resulting wavelet coefficient field of a target image function ρ is defined by $\zeta = \left((\zeta_{a,k})_{1 \leq k \leq K_{j_{\max}}}, (\zeta_{o,j,k})_{1 \leq j \leq j_{\max}, 1 \leq k \leq K_j}\right)$ where $K_j = K2^{-2j}$ is the number of wavelet coefficients in a given subband at resolution j (by assuming that Y and X are multiple of $2^{j_{\max}}$) and the coefficients have been reindexed in such a way that $\zeta_{a,k}$ denotes an approximation coefficient at resolution level $j_{\max}$ and $\zeta_{o,j,k}$ denotes a detail coefficient at resolution level j and orientation $o \in \{h, v, d\}$ (h, v and d stand for *horizontal*, *vertical* and *diagonal*, respectively). From a Bayesian viewpoint, regularization consists of injecting some a priori knowledge about the optimal solution. The computation of the minimizer of $\mathcal{J}$ therefore consists of finding the Maximum a Posteriori (MAP) solution based on the likelihood and the prior distribution. In our case, this prior involves $\overline{\zeta} = T\overline{\rho}$, the forward WT of the sought image $\overline{\rho}$. Here, we assume that the probability density function (pdf) of the corresponding real and imaginary parts of the wavelet coefficients ζ is a generalized Gaussian distribution (GG). Hence, for each coefficient ξ in a given sub-band $\zeta_{o,j,k}$ ($o \in \{a, h, v, d\}$), the neg-log prior pdf is given by

$$\begin{aligned}\Phi_{o,j}(\xi) =& \Phi^{\mathrm{Re}}_{o,j}(\xi) + \Phi^{\mathrm{Im}}_{o,j}(\xi) \\ =& (\omega^{\mathrm{Re}}_{o,j}|\mathrm{Re}(\xi)|)^{\beta^{\mathrm{Re}}_{o,j}} + (\omega^{\mathrm{Im}}_{o,j}|\mathrm{Im}(\xi)|)^{\beta^{\mathrm{Im}}_{o,j}} \end{aligned} \quad (5)$$

Hereabove, $\mathrm{Re}(\cdot)$ and $\mathrm{Im}(\cdot)$ (or $\cdot^{\mathrm{Re}}$ and $\cdot^{\mathrm{Im}}$) stand for the real and imaginary parts, respectively. Note that $(\omega^{\mathrm{Re}}_{o,j}, \omega^{\mathrm{Im}}_{o,j}) \in \mathbb{R}^2_+$, $\beta^{\mathrm{Re}}_{o,j} \geq 1$ and $\beta^{\mathrm{Im}}_{o,j} \geq 1$ are hyperparameters, which have to be estimated. In [6], we automatically tune these statistical parameters in the maximum likelihood sense on the SENSE-based reconstructed image. In order to achieve more robust reconstruction and avoid noise outside the brain mask, another penalty may be considered in the regularization term. This additional prior is simply an indicator function $i_{\mathcal{M}}$ on the brain mask $\mathcal{M}$ [3]. When $\kappa_1 = \kappa_2 = 1$, the criterion in Eq. (3) writes:

$$\mathcal{J}_{\mathrm{WT}}(\rho) = \sum_{\mathbf{r}} \| \boldsymbol{d}(\boldsymbol{r}) - \boldsymbol{S}(\boldsymbol{r})\boldsymbol{\rho}(\boldsymbol{r}) \|^2_{\boldsymbol{\Psi}^{-1}} + \Phi(T\rho) + i_{\mathcal{M}}(\rho),$$

where $\Phi(T\rho) = \sum_k \Phi_a((T\rho)_{a,k}) + \sum_o \sum_j \sum_k \Phi_{o,j}((T\rho)_{o,j,k})$. Although this criterion is convex and admits a global minimizer, it cannot be optimized using standard algorithms like pseudo-conjugate gradient since it is not differentiable. To address this problem, many recent algorithms have been proposed in the convex optimization literature dealing with non-differentiable criteria like FISTA [10] or Forward-Backward [11]. However, most of them are designed for solving convex criteria including only the sum of two functions, whereas our criterion is the sum of three convex functions. For this reason, we will use the PPXA algorithm [12] which enables the optimization of $m \in \mathbb{N}$ functions, provided that, for each of them the proximity operator admits a closed form expression [12]. To summarize, our methodological contribution also called 1D-UWR-SENSE algorithm minimizes the regularized criterion $\mathcal{J}_{\mathrm{WT}}$ using the PPXA algorithm. The PPXA parameters have to be well adjusted to ensure faster convergence [12].

[3] $\forall \rho \in \mathbb{C}^K, i_{\mathcal{M}}(\rho) = \sum_{\boldsymbol{r}} i_0(\rho(\boldsymbol{r}))$ where $i_0(\rho(\boldsymbol{r})) = 0$ if $\boldsymbol{r} \in \mathcal{M}$ and $+\infty$ otherwise

4 Results

The fMRI data were recorded at 3 Tesla on a Siemens Trio magnet using a Gradient-Echo EPI (GE-EPI) sequence ($TE = 30$ ms, $TR = 2,4$ s, slice thickness = 3 mm, transversal orientation, FoV = 192 mm^2) during a cognitive localizer experiment designed to map auditory, visual and motor brain functions as well as higher cognitive tasks such as number processing and language comprehension. It consisted of a single session of $N = 128$ scans. The paradigm was a fast event-related design comprising sixty auditory, visual and motor stimuli, defined in ten experimental conditions (auditory and visual sentences, auditory and visual calculations, left/right auditory and visual clicks, horizontal and vertical checkerboards). A $L = 32$ channels coil was used to enable parallel imaging. Eighteen subjects gave informed consent to be scanned. In each subject, fMRI data were collected at different in-plane spatial resolutions (3×3 and 2×2 mm^2). The mSENSE algorithm available on the Siemens workstation was used with varying the acceleration factor ($R = 2$ or $R = 4$).

4.1 Reconstruction comparison

All acquired data were first reconstructed using the black-box Siemens pipeline available on the Workstation. Since we also recorded the *raw* or un-reconstructed data, we enabled the comparison with our own reconstruction pipeline, which proceeds as follows for EPI images: *(i)*: k-space regridding to take into account non-uniform k space sampling, which occurs in fast MRI sequences like GE-EPI; *(ii)* Removal of EPI Nyquist ghost artifacts due to the odd-even echo inconsistencies; *(iii)* Estimation of the sensitivity maps based upon an acquisition of the k-space center (24 lines) before the N scans. *(iv)* L single channel reduced FoV reconstructions

by inverse Fourier transform on corrected EPI images. *(vi)* Perform 1D-UWR-SENSE reconstruction for each scan separately (parallel processing). In a eight-CPU computer (Intel Xeon `W3520@2.67GHz`), the complete procedure takes about 2h30, by loading the reconstruction of 16 scans per CPU. However, for comparison purpose, Fig. 1 shows typical examples of reconstructed images using mSENSE and 1D-UWR-SENSE algorithms for $R = 2$ and $R = 4$ with $2 \times 2\text{mm}^2$ in-plane resolution.

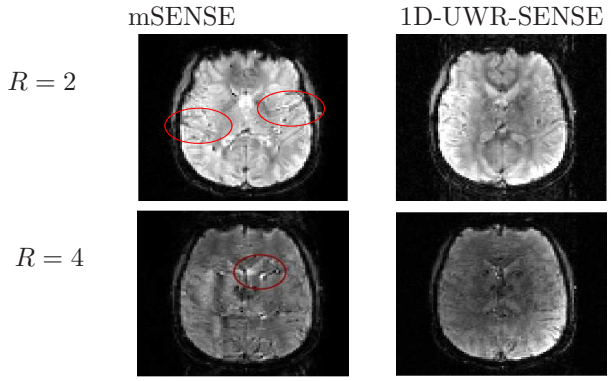

Fig. 1. Reconstructed slice using mSENSE and 1D-UWR-SENSE for $R = 2$ and $R = 4$ with $2 \times 2\text{mm}^2$ in-plane resolution. Radiological convention: left is right.

Through illustrated images, it is clear that 1D-UWR-SENSE provides better full FoV images than mSENSE. In Fig. 1 ($R = 2$), it is shown that mSENSE generates strong artifacts in the right temporal lobe (on the left side) and in the left frontal lobe (on the right side) of the slice, while our 1D-UWR-SENSE still gives quite accurate reconstruction. At $R = 4$, it is also clear that the mSENSE algorithm induces strong artifacts close to the deep cerebellar nuclei, which are completely removed using our algorithm. Note that these conclusions are reproducible across subjects.

4.2 Impact on brain activity detection

Also, we quantitatively compare the performance of mSENSE and 1D-UWR-SENSE pMRI reconstruction algorithms for brain activity detection at the subject-level on $2 \times 2 \times 3\text{mm}^3$ EPI data. fMRI data analysis has been conducted using the GLM framework proposed in SPM5 in which the design matrix shown in Figs. 2-3 relying on ten regressors has been built up. Here, we only report results involving the Visual vs. Checkerboard (`V-C`) and Auditory vs. Visual (`A-V`) contrasts since the expected activations, which lie in different parts of the brain, can be putatively corrupted by reconstruction artifacts. The results are reported in terms of Student-t statistical maps thresholded at a $p = 0.05$ p-value corrected for multiple comparisons [13] as well as statistical tables that provide cluster- and voxel-level p-values, maximal T-scores and corresponding locations of these peaks. In Fig. 2, it is shown that the 1D-UWR-SENSE approach enables the recovery of expected bilateral activations in the temporal lobes elicited by speech perception and comprehension involved in the `A-V` contrast, while the mSENSE method retrieved smaller clusters: activation cluster in the left hemisphere is somehow lost due to strong reconstruction artifacts. This result holds both for $R = 2$ and $R = 4$. From a quantitative point of view, our approach recovers larger clusters whose excursion or local maxima is close to the one obtained using mSENSE. Concerning the largest clusters, our approach gives always the highest T-score of the local maxima (see Table 1). The `A-V` contrast defines a compound comparison which involves the same stimuli presented either in the visual or auditory modality, respectively. In this sense, this comparison aims only at localizing sensory brain areas, i.e. the primary auditory cortices.

For the `V-C` contrast, Fig. 3 shows that the 1D-UWR-SENSE algorithm allows the detection of expected activated areas missed by the mSENSE algorithm, both for $R = 2$ and $R = 4$. Quantitative results in Table 1 show that larger clusters with higher local T-scores maxima are detected using our approach, both at $R = 2$ and $R = 4$. The visual condition comprises both visual sentence and checkerboard. Subtracting checkerboard to visual stimuli illustrates activation to reading processing and comprehension in the left temporal lobe.

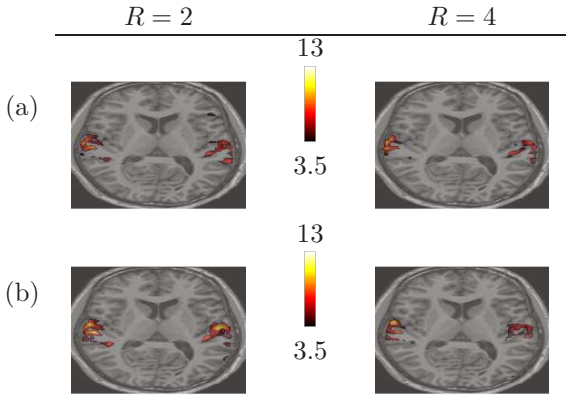

Fig. 2. Student-t maps superimposed to anatomical MRI for the `A-V` contrast: (a): mSENSE algorithm; (b): 1D-UWR-SENSE algorithm (left is right).

5 Conclusion

In this contribution, we examined the impact of the pMRI reconstruction algorithm on the statistical performance for brain activity detection in BOLD fMRI. At the subject-level, we showed that our 1D-UWR-SENSE algorithm outperforms the mSENSE algorithm both qualitatively and quantitatively from a statistical viewpoint. Also, we illustrated that the choice of the pMRI reconstruction algorithm enables whole brain neuroscience studies at high spatial resolution. Fu-

Table 1. Significant statistical results for the `V-C` contrast.

		1D-UWR-SENSE				mSENSE			
		cluster-level		voxel-level		cluster-level		voxel-level	
		p-value	Size	T-score	Position	p-value	Size	T-score	Position
A-V	$R=2$	$< 10^{-3}$	**847**	**10.82**	**-52 -12 3**	$< 10^{-3}$	668	10.16	-52 -38 15
		$< 10^{-3}$	804	11.37	60 -20 9	$< 10^{-3}$	666	11.54	64 -8 3
	$R=4$	$< 10^{-3}$	**353**	**9.89**	**-62 -38 15**	$< 10^{-3}$	251	8.91	-66 -40 12
		$< 10^{-3}$	147	8.99	62 -6 6	$< 10^{-3}$	204	9.17	64 -8 6
V-C	$R=2$	$< 10^{-3}$	**110**	**6.49**	**-60 -16 27**	12×10^{-3}	27	4.22	-62 -42 6
		6×10^{-3}	32	6.26	-30 -82 -12	1×10^{-3}	42	6.85	-30 -84 -12
	$R=4$	$< 10^{-3}$	**89**	**6.21**	**-52 -16 27**	$< 10^{-3}$	51	5.95	-62 -22 21
		$< 10^{-3}$	43	4.57	-50 2 33	$< 10^{-3}$	48	5.37	-50 4 33

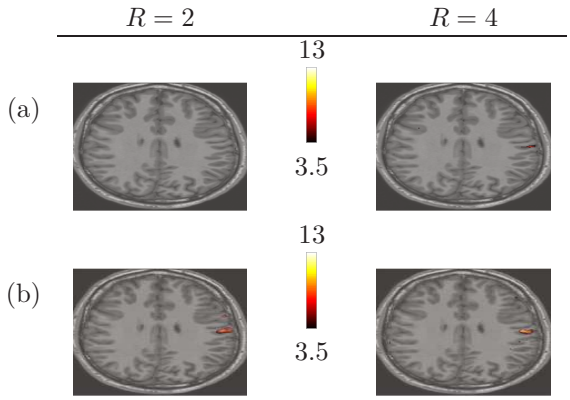

Fig. 3. Student-t maps superimposed to anatomical MRI for the `V-C` contrast: (a): mSENSE algorithm; (b): 1D-UWR-SENSE algorithm: radiological convention: left is right.

ture work will concern the statistical comparison at the group-level, as well as the impact of varying the in-plane resolution. Post-modern fMRI data analysis will then be achieved combining 1D-UWR-SENSE reconstruction and joint detection estimation of brain activity in the volume [14–16] or along the cortical surface [17].

6 References

[1] M. A. Griswold, P. M. Jakob, R. M. Heidemann, M. Nittka, V. Jellus, J. Wang, B. Kiefer, and A. Haase, "Generalized autocalibrating partially parallel acquisitions GRAPPA," *Mag. Res. in Med.*, vol. 47, no. 6, pp. 1202–1210, Jun. 2002.

[2] K. P. Pruessmann, M. Weiger, M. B. Scheidegger, and P. Boesiger, "SENSE: sensitivity encoding for fast MRI," *Mag. Res. in Med.*, vol. 42, no. 5, pp. 952–962, Jul. 1999.

[3] Z. P. Liang, R. Bammer, J. Ji, N. J. Pelc, and G. H. Glover, "Making better SENSE: wavelet denoising, Tikhonov regularization, and total least squares," in *ISMRMM*, Hawaï, USA, May 18-24 2002, p. 2388.

[4] L. Ying, D. Xu, and Z.-P. Liang, "On Tikhonov Regularization for image reconstruction in parallel MRI," in *IEEE EMBS*, San Francisco, USA, Sept. 1-5 2004, pp. 1056–1059.

[5] Y. M. Zou, L. Ying, and B. Liu, "SparseSENSE: application of compressed sensing in parallel MRI," in *IEEE ICTAB*, Shenzhen, China, May 30-31 2008, pp. 127–130.

[6] L. Chaâri, J.-C. Pesquet, A. Benazza-Benyahia, and Ph. Ciuciu, "Autocalibrated parallel MRI reconstruction in the wavelet domain," in *IEEE ISBI*, Paris, France, May 14-17 2008, pp. 756–759.

[7] B. Liu, E. Abdelsalam, J. Sheng, and L. Ying, "Improved spiral SENSE reconstruction using a multiscale wavelet model," in *IEEE ISBI*, Paris, France, May 14-17 2008, pp. 1505–1508.

[8] L. Chaâri, J.-C. Pesquet, A. Benazza-Benyahia, and Ph. Ciuciu, "A wavelet-based regularized reconstruction algorithm for SENSE parallel MRI with applications to neuroimaging," *Medical Image Analysis*, 2010, In press.

[9] C. Rabrait, Ph. Ciuciu, A. Ribès, C. Poupon, P. Leroux, V. Lebon, G. Dehaene-Lambertz, D. Le Bihan, and F. Lethimonnier, "High temporal resolution functional MRI using parallel echo volume imaging," *Mag. Res. in Med.*, vol. 27, no. 4, pp. 744–753, Mar. 2008.

[10] A. Beck and M. Teboulle, "A Fast Iterative Shrinkage-Thresholding Algorithm for Linear Inverse Problems," *SIAM Journal on Imaging Sciences*, vol. 2, no. 1, pp. 183–202, 2009.

[11] C. Chaux, P. Combettes, J.-C. Pesquet, and V.R Wajs, "A variational formulation for frame-based inverse problems," *Inv. Problems*, vol. 23, no. 4, pp. 1495–1518, Aug. 2007.

[12] P. L. Combettes and J.-C. Pesquet, "A proximal decomposition method for solving convex variational inverse problems," *Inv. Problems*, vol. 24, no. 6, 2009.

[13] J. Ashburner, K. J. Friston, and W. Penny, *Human Brain Function, J. Ashburner, K. Friston and W. Penny Eds*, chapter Introduction to Random Field Theory, Academic Press, 2nd edition, 2004.

[14] S. Makni, J. Idier, T. Vincent, B. Thirion, G. Dehaene-Lambertz, and P. Ciuciu, "A fully Bayesian approach to the parcel-based detection-estimation of brain activity in fMRI," *Neuroimage*, vol. 41, no. 3, pp. 941–969, 2008.

[15] L. Risser, T. Vincent, P. Ciuciu, and J. Idier, "Robust extrapolation scheme for fast estimation of 3D Ising field partition functions. application to within-subject fMRI data analysis.," in *12thProc. MICCAI'09*, G.-Z. Yang, Ed., London, UK, Sep 2009, LNCS 5761, pp. 975–983, Springer Verlag.

[16] T. Vincent, L. Risser, and P. Ciuciu, "Spatially adaptive mixture modeling for analysis of within-subject fMRI time series," *IEEE Trans. Med. Imag.*, vol. 29, no. 4, pp. 1059–1074, 2010.

[17] Christophe Grova, Salima Makni, G. Flandin, P. Ciuciu, J. Gotman, and J.-B. Poline, "Anatomically informed interpolation of fMRI data on the cortical surface," *Neuroimage*, vol. 31, pp. 1475–1486, 2006.